EUROPEAN ORGANIZATION FOR NUCLEAR RESEARCH

CERN–EP/99–59

19 April 1999

A search for invisible Higgs bosons produced in e^+e^- interactions at LEP 2 energies

DELPHI Collaboration

Abstract

Searches for HZ production with the Higgs boson decaying into an invisible final state have been performed with the data collected by the DELPHI experiment up to the centre-of-mass energy of 183 GeV. The hadronic and muon pair final states of the Z boson were analysed. From the absence of signal, upper limits on the cross-section and the corresponding Higgs boson mass limits were set at 95% confidence level. The results are interpreted as excluded parameter regions in the framework of the minimal supersymmetric standard model and in the simplest Majoron model with one Higgs doublet and one Higgs singlet field.

(Accepted by Phys. Lett. B)

P.Abreu[21], W.Adam[50], T.Adye[36], P.Adzic[11], Z.Albrecht[17], T.Alderweireld[2], G.D.Alekseev[16], R.Alemany[49], T.Allmendinger[17], P.P.Allport[22], S.Almehed[24], U.Amaldi[9], N.Amapane[45], S.Amato[47], E.G.Anassontzis[3], P.Andersson[44], A.Andreazza[9], S.Andringa[21], P.Antilogus[25], W-D.Apel[17], Y.Arnoud[9], B.Åsman[44], J-E.Augustin[25], A.Augustinus[9], P.Baillon[9], P.Bambade[19], F.Barao[21], G.Barbiellini[46], R.Barbier[25], D.Y.Bardin[16], G.Barker[17], A.Baroncelli[38], M.Battaglia[15], M.Baubillier[23], K-H.Becks[52], M.Begalli[6], A.Behrmann[52], P.Beilliere[8], Yu.Belokopytov[9,53], K.Belous[42], N.C.Benekos[31], A.C.Benvenuti[5], C.Berat[14], M.Berggren[25], D.Bertini[25], D.Bertrand[2], M.Besancon[39], M.Bigi[45], M.S.Bilenky[16], M-A.Bizouard[19], D.Bloch[10], H.M.Blom[30], M.Bonesini[27], W.Bonivento[27], M.Boonekamp[39], P.S.L.Booth[22], A.W.Borgland[4], G.Borisov[19], C.Bosio[41], O.Botner[48], E.Boudinov[30], B.Bouquet[19], C.Bourdarios[19], T.J.V.Bowcock[22], I.Boyko[16], I.Bozovic[11], M.Bozzo[13], P.Branchini[38], T.Brenke[52], R.A.Brenner[48], P.Bruckman[18], J-M.Brunet[8], L.Bugge[32], T.Buran[32], T.Burgsmueller[52], B.Buschbeck[50], P.Buschmann[52], S.Cabrera[49], M.Caccia[27], M.Calvi[27], T.Camporesi[9], V.Canale[37], F.Carena[9], L.Carroll[22], C.Caso[13], M.V.Castillo Gimenez[49], A.Cattai[9], F.R.Cavallo[5], V.Chabaud[9], M.Chapkin[42], Ph.Charpentier[9], L.Chaussard[25], P.Checchia[35], G.A.Chelkov[16], R.Chierici[45], P.Chliapnikov[42], P.Chochula[7], V.Chorowicz[25], J.Chudoba[29], K.Cieslik[18], P.Collins[9], R.Contri[13], E.Cortina[49], G.Cosme[19], F.Cossutti[9], J-H.Cowell[22], H.B.Crawley[1], D.Crennell[36], S.Crepe[14], G.Crosetti[13], J.Cuevas Maestro[33], S.Czellar[15], M.Davenport[9], W.Da Silva[23], A.Deghorain[2], G.Della Ricca[46], P.Delpierre[26], N.Demaria[9], A.De Angelis[9], W.De Boer[17], C.De Clercq[2], B.De Lotto[46], A.De Min[35], L.De Paula[47], H.Dijkstra[9], L.Di Ciaccio[37,9], J.Dolbeau[8], K.Doroba[51], M.Dracos[10], J.Drees[52], M.Dris[31], A.Duperrin[25], J-D.Durand[9], G.Eigen[4], T.Ekelof[48], G.Ekspong[44], M.Ellert[48], M.Elsing[9], J-P.Engel[10], B.Erzen[43], M.Espirito Santo[21], E.Falk[24], G.Fanourakis[11], D.Fassouliotis[11], J.Fayot[23], M.Feindt[17], A.Fenyuk[42], P.Ferrari[27], A.Ferrer[49], E.Ferrer-Ribas[19], F.Ferro[13], S.Fichet[23], A.Firestone[1], U.Flagmeyer[52], H.Foeth[9], E.Fokitis[31], F.Fontanelli[13], B.Franek[36], A.G.Frodesen[4], R.Fruhwirth[50], F.Fulda-Quenzer[19], J.Fuster[49], A.Galloni[22], D.Gamba[45], S.Gamblin[19], M.Gandelman[47], C.Garcia[49], C.Gaspar[9], M.Gaspar[47], U.Gasparini[35], Ph.Gavillet[9], E.N.Gazis[31], D.Gele[10], N.Ghodbane[25], I.Gil[49], F.Glege[52], R.Gokieli[9,51], B.Golob[43], G.Gomez-Ceballos[40], P.Goncalves[21], I.Gonzalez Caballero[40], G.Gopal[36], L.Gorn[1,54], M.Gorski[51], Yu.Gouz[42], V.Gracco[13], J.Grahl[1], E.Graziani[38], C.Green[22], H-J.Grimm[17], P.Gris[39], G.Grosdidier[19], K.Grzelak[51], M.Gunther[48], J.Guy[36], F.Hahn[9], S.Hahn[52], S.Haider[9], A.Hallgren[48], K.Hamacher[52], J.Hansen[32], F.J.Harris[34], V.Hedberg[24], S.Heising[17], J.J.Hernandez[49], P.Herquet[2], H.Herr[9], T.L.Hessing[34], J.-M.Heuser[52], E.Higon[49], S-O.Holmgren[44], P.J.Holt[34], S.Hoorelbeke[2], M.Houlden[22], J.Hrubec[50], K.Huet[2], G.J.Hughes[22], K.Hultqvist[44], J.N.Jackson[22], R.Jacobsson[9], P.Jalocha[9], R.Janik[7], Ch.Jarlskog[24], G.Jarlskog[24], P.Jarry[39], B.Jean-Marie[19], E.K.Johansson[44], P.Jonsson[25], C.Joram[9], P.Juillot[10], F.Kapusta[23], K.Karafasoulis[11], S.Katsanevas[25], E.C.Katsoufis[31], R.Keranen[17], B.P.Kersevan[43], B.A.Khomenko[16], N.N.Khovanski[16], A.Kiiskinen[15], B.King[22], A.Kinvig[22], N.J.Kjaer[30], O.Klapp[52], H.Klein[9], P.Kluit[30], P.Kokkinias[11], M.Koratzinos[9], V.Kostioukhine[42], C.Kourkoumelis[3], O.Kouznetsov[39], M.Krammer[50], E.Kriznic[43], J.Krstic[11], Z.Krumstein[16], P.Kubinec[7], J.Kurowska[51], K.Kurvinen[15], J.W.Lamsa[1], D.W.Lane[1], P.Langefeld[52], V.Lapin[42], J-P.Laugier[39], R.Lauhakangas[15], G.Leder[50], F.Ledroit[14], V.Lefebure[2], L.Leinonen[44], A.Leisos[11], R.Leitner[29], J.Lemonne[2], G.Lenzen[52], V.Lepeltier[19], T.Lesiak[18], M.Lethuillier[39], J.Libby[34], D.Liko[9], A.Lipniacka[44], I.Lippi[35], B.Loerstad[24], J.G.Loken[34], J.H.Lopes[47], J.M.Lopez[40], R.Lopez-Fernandez[14], D.Loukas[11], P.Lutz[39], L.Lyons[34], J.MacNaughton[50], J.R.Mahon[6], A.Maio[21], A.Malek[52], T.G.M.Malmgren[44], S.Maltezos[31], V.Malychev[16], F.Mandl[50], J.Marco[40], R.Marco[40], B.Marechal[47], M.Margoni[35], J-C.Marin[9], C.Mariotti[9], A.Markou[11], C.Martinez-Rivero[19], F.Martinez-Vidal[49], S.Marti i Garcia[9], J.Masik[12], N.Mastroyiannopoulos[11], F.Matorras[40], C.Matteuzzi[27], G.Matthiae[37], F.Mazzucato[35], M.Mazzucato[35], M.Mc Cubbin[22], R.Mc Kay[1], R.Mc Nulty[22], G.Mc Pherson[22], C.Meroni[27], W.T.Meyer[1], E.Migliore[45], L.Mirabito[25], W.A.Mitaroff[50], U.Mjoernmark[24], T.Moa[44], M.Moch[17], R.Moeller[28], K.Moenig[9], M.R.Monge[13], X.Moreau[23], P.Morettini[13], G.Morton[34], U.Mueller[52], K.Muenich[52], M.Mulders[30], C.Mulet-Marquis[14], R.Muresan[24], W.J.Murray[36], B.Muryn[14,18], G.Myatt[34], T.Myklebust[32], F.Naraghi[14], M.Nassiakou[11], F.L.Navarria[5], S.Navas[49], K.Nawrocki[51], P.Negri[27], S.Nemecek[12], N.Neufeld[9], N.Neumeister[50], R.Nicolaidou[39], B.S.Nielsen[28], M.Nikolenko[10,16], V.Nomokonov[15], A.Normand[22], A.Nygren[24], V.Obraztsov[42], A.G.Olshevski[16], A.Onofre[21], R.Orava[15], G.Orazi[10], K.Osterberg[15], A.Ouraou[39], M.Paganoni[27], S.Paiano[5], R.Pain[23], R.Paiva[21], J.Palacios[34], H.Palka[18], Th.D.Papadopoulou[31,9], K.Papageorgiou[11], L.Pape[9], C.Parkes[9], F.Parodi[13], U.Parzefall[22], A.Passeri[38], O.Passon[52], M.Pegoraro[35], L.Peralta[21], M.Pernicka[50], A.Perrotta[5], C.Petridou[46], A.Petrolini[13], H.T.Phillips[36], F.Pierre[39], M.Pimenta[21], E.Piotto[27], T.Podobnik[43], M.E.Pol[6], G.Polok[18], P.Poropat[46], V.Pozdniakov[16], P.Privitera[37], N.Pukhaeva[16], A.Pullia[27], D.Radojicic[34], S.Ragazzi[27], H.Rahmani[31], P.N.Ratoff[20], A.L.Read[32], P.Rebecchi[9], N.G.Redaelli[27], D.Reid[30], R.Reinhardt[52], P.B.Renton[34], L.K.Resvanis[3], F.Richard[19], J.Ridky[12], G.Rinaudo[45], O.Rohne[32], A.Romero[45], P.Ronchese[35], E.I.Rosenberg[1], P.Rosinsky[7], P.Roudeau[19], T.Rovelli[5], Ch.Royon[39], V.Ruhlmann-Kleider[39], A.Ruiz[40], H.Saarikko[15], Y.Sacquin[39], A.Sadovsky[16], G.Sajot[14], J.Salt[49], D.Sampsonidis[11], M.Sannino[13], H.Schneider[17], Ph.Schwemling[23], B.Schwering[52], U.Schwickerath[17], M.A.E.Schyns[52], F.Scuri[46], P.Seager[20], Y.Sedykh[16], A.M.Segar[34], R.Sekulin[36], R.C.Shellard[6], A.Sheridan[22], M.Siebel[52], L.Simard[39], F.Simonetto[35], A.N.Sisakian[16], G.Smadja[25], N.Smirnov[42], O.Smirnova[24], G.R.Smith[36], A.Sopczak[17], R.Sosnowski[51], T.Spassov[21], E.Spiriti[38], P.Sponholz[52], S.Squarcia[13], C.Stanescu[38], S.Stanic[43], K.Stevenson[34], A.Stocchi[19], J.Strauss[50], R.Strub[10], B.Stugu[4], M.Szczekowski[51], M.Szeptycka[51], T.Tabarelli[27], F.Tegenfeldt[48], F.Terranova[27], J.Thomas[34], J.Timmermans[30], N.Tinti[5], L.G.Tkatchev[16], S.Todorova[10], A.Tomaradze[2], B.Tome[21], A.Tonazzo[9], L.Tortora[38],

G.Transtromer[24], D.Treille[9], G.Tristram[8], M.Trochimczuk[51], C.Troncon[27], A.Tsirou[9], M-L.Turluer[39], I.A.Tyapkin[16], S.Tzamarias[11], O.Ullaland[9], V.Uvarov[42], G.Valenti[5], E.Vallazza[46], C.Vander Velde[2], G.W.Van Apeldoorn[30], P.Van Dam[30], W.K.Van Doninck[2], J.Van Eldik[30], A.Van Lysebetten[2], N.Van Remortel[2], I.Van Vulpen[30], N.Vassilopoulos[34], G.Vegni[27], L.Ventura[35], W.Venus[36,9], F.Verbeure[2], M.Verlato[35], L.S.Vertogradov[16], V.Verzi[37], D.Vilanova[39], L.Vitale[46], E.Vlasov[42], A.S.Vodopyanov[16], C.Vollmer[17], G.Voulgaris[3], V.Vrba[12], H.Wahlen[52], C.Walck[44], C.Weiser[17], D.Wicke[52], J.H.Wickens[2], G.R.Wilkinson[9], M.Winter[10], M.Witek[18], G.Wolf[9], J.Yi[1], O.Yushchenko[42], A.Zaitsev[42], A.Zalewska[18], P.Zalewski[51], D.Zavrtanik[43], E.Zevgolatakos[11], N.I.Zimin[16,24], G.C.Zucchelli[44], G.Zumerle[35]

[1]Department of Physics and Astronomy, Iowa State University, Ames IA 50011-3160, USA
[2]Physics Department, Univ. Instelling Antwerpen, Universiteitsplein 1, BE-2610 Wilrijk, Belgium
and IIHE, ULB-VUB, Pleinlaan 2, BE-1050 Brussels, Belgium
and Faculté des Sciences, Univ. de l'Etat Mons, Av. Maistriau 19, BE-7000 Mons, Belgium
[3]Physics Laboratory, University of Athens, Solonos Str. 104, GR-10680 Athens, Greece
[4]Department of Physics, University of Bergen, Allégaten 55, NO-5007 Bergen, Norway
[5]Dipartimento di Fisica, Università di Bologna and INFN, Via Irnerio 46, IT-40126 Bologna, Italy
[6]Centro Brasileiro de Pesquisas Físicas, rua Xavier Sigaud 150, BR-22290 Rio de Janeiro, Brazil
and Depto. de Física, Pont. Univ. Católica, C.P. 38071 BR-22453 Rio de Janeiro, Brazil
and Inst. de Física, Univ. Estadual do Rio de Janeiro, rua São Francisco Xavier 524, Rio de Janeiro, Brazil
[7]Comenius University, Faculty of Mathematics and Physics, Mlynska Dolina, SK-84215 Bratislava, Slovakia
[8]Collège de France, Lab. de Physique Corpusculaire, IN2P3-CNRS, FR-75231 Paris Cedex 05, France
[9]CERN, CH-1211 Geneva 23, Switzerland
[10]Institut de Recherches Subatomiques, IN2P3 - CNRS/ULP - BP20, FR-67037 Strasbourg Cedex, France
[11]Institute of Nuclear Physics, N.C.S.R. Demokritos, P.O. Box 60228, GR-15310 Athens, Greece
[12]FZU, Inst. of Phys. of the C.A.S. High Energy Physics Division, Na Slovance 2, CZ-180 40, Praha 8, Czech Republic
[13]Dipartimento di Fisica, Università di Genova and INFN, Via Dodecaneso 33, IT-16146 Genova, Italy
[14]Institut des Sciences Nucléaires, IN2P3-CNRS, Université de Grenoble 1, FR-38026 Grenoble Cedex, France
[15]Helsinki Institute of Physics, HIP, P.O. Box 9, FI-00014 Helsinki, Finland
[16]Joint Institute for Nuclear Research, Dubna, Head Post Office, P.O. Box 79, RU-101 000 Moscow, Russian Federation
[17]Institut für Experimentelle Kernphysik, Universität Karlsruhe, Postfach 6980, DE-76128 Karlsruhe, Germany
[18]Institute of Nuclear Physics and University of Mining and Metalurgy, Ul. Kawiory 26a, PL-30055 Krakow, Poland
[19]Université de Paris-Sud, Lab. de l'Accélérateur Linéaire, IN2P3-CNRS, Bât. 200, FR-91405 Orsay Cedex, France
[20]School of Physics and Chemistry, University of Lancaster, Lancaster LA1 4YB, UK
[21]LIP, IST, FCUL - Av. Elias Garcia, 14-1^o, PT-1000 Lisboa Codex, Portugal
[22]Department of Physics, University of Liverpool, P.O. Box 147, Liverpool L69 3BX, UK
[23]LPNHE, IN2P3-CNRS, Univ. Paris VI et VII, Tour 33 (RdC), 4 place Jussieu, FR-75252 Paris Cedex 05, France
[24]Department of Physics, University of Lund, Sölvegatan 14, SE-223 63 Lund, Sweden
[25]Université Claude Bernard de Lyon, IPNL, IN2P3-CNRS, FR-69622 Villeurbanne Cedex, France
[26]Univ. d'Aix - Marseille II - CPP, IN2P3-CNRS, FR-13288 Marseille Cedex 09, France
[27]Dipartimento di Fisica, Università di Milano and INFN, Via Celoria 16, IT-20133 Milan, Italy
[28]Niels Bohr Institute, Blegdamsvej 17, DK-2100 Copenhagen Ø, Denmark
[29]NC, Nuclear Centre of MFF, Charles University, Areal MFF, V Holesovickach 2, CZ-180 00, Praha 8, Czech Republic
[30]NIKHEF, Postbus 41882, NL-1009 DB Amsterdam, The Netherlands
[31]National Technical University, Physics Department, Zografou Campus, GR-15773 Athens, Greece
[32]Physics Department, University of Oslo, Blindern, NO-1000 Oslo 3, Norway
[33]Dpto. Fisica, Univ. Oviedo, Avda. Calvo Sotelo s/n, ES-33007 Oviedo, Spain
[34]Department of Physics, University of Oxford, Keble Road, Oxford OX1 3RH, UK
[35]Dipartimento di Fisica, Università di Padova and INFN, Via Marzolo 8, IT-35131 Padua, Italy
[36]Rutherford Appleton Laboratory, Chilton, Didcot OX11 OQX, UK
[37]Dipartimento di Fisica, Università di Roma II and INFN, Tor Vergata, IT-00173 Rome, Italy
[38]Dipartimento di Fisica, Università di Roma III and INFN, Via della Vasca Navale 84, IT-00146 Rome, Italy
[39]DAPNIA/Service de Physique des Particules, CEA-Saclay, FR-91191 Gif-sur-Yvette Cedex, France
[40]Instituto de Fisica de Cantabria (CSIC-UC), Avda. los Castros s/n, ES-39006 Santander, Spain
[41]Dipartimento di Fisica, Università degli Studi di Roma La Sapienza, Piazzale Aldo Moro 2, IT-00185 Rome, Italy
[42]Inst. for High Energy Physics, Serpukov P.O. Box 35, Protvino, (Moscow Region), Russian Federation
[43]J. Stefan Institute, Jamova 39, SI-1000 Ljubljana, Slovenia and Laboratory for Astroparticle Physics,
Nova Gorica Polytechnic, Kostanjeviska 16a, SI-5000 Nova Gorica, Slovenia,
and Department of Physics, University of Ljubljana, SI-1000 Ljubljana, Slovenia
[44]Fysikum, Stockholm University, Box 6730, SE-113 85 Stockholm, Sweden
[45]Dipartimento di Fisica Sperimentale, Università di Torino and INFN, Via P. Giuria 1, IT-10125 Turin, Italy
[46]Dipartimento di Fisica, Università di Trieste and INFN, Via A. Valerio 2, IT-34127 Trieste, Italy
and Istituto di Fisica, Università di Udine, IT-33100 Udine, Italy
[47]Univ. Federal do Rio de Janeiro, C.P. 68528 Cidade Univ., Ilha do Fundão BR-21945-970 Rio de Janeiro, Brazil
[48]Department of Radiation Sciences, University of Uppsala, P.O. Box 535, SE-751 21 Uppsala, Sweden
[49]IFIC, Valencia-CSIC, and D.F.A.M.N., U. de Valencia, Avda. Dr. Moliner 50, ES-46100 Burjassot (Valencia), Spain
[50]Institut für Hochenergiephysik, Österr. Akad. d. Wissensch., Nikolsdorfergasse 18, AT-1050 Vienna, Austria
[51]Inst. Nuclear Studies and University of Warsaw, Ul. Hoza 69, PL-00681 Warsaw, Poland
[52]Fachbereich Physik, University of Wuppertal, Postfach 100 127, DE-42097 Wuppertal, Germany
[53]On leave of absence from IHEP Serpukhov
[54]Now at University of Florida

1 Introduction

This paper presents a search for the production of $e^+e^- \rightarrow HZ$, with $Z \rightarrow q\bar{q}$ or $\mu^+\mu^-$ and the Higgs boson decaying into stable non-interacting particles rendering it invisible (see fig. 1). The search was carried out with the data accumulated by DELPHI at $\sqrt{s} \simeq 183$ GeV. The DELPHI analyses at $\sqrt{s} =$ 161-172 GeV [1] have been taken into account in deriving the results. The other LEP experiments have also performed searches in this channel [2].

The process being studied is possible in the Minimal Supersymmetric Model (MSSM) [3] when Higgs decaying into neutralinos $\tilde{\chi}_1^0$ are open and R-parity is conserved, i.e. the lightest supersymmetric particle (LSP) is $\tilde{\chi}_1^0$ which is stable and invisible. Detailed information about these decay modes can be found in [4]. Invisible Higgs boson decay modes can be envisaged in other supersymmetric [5] and non-supersymmetric extensions of the Standard Model (SM). The Majoron-type models [7,8] are taken here as a specific example. The characteristic feature of these models is the presence of complex SU(2)×U(1) singlet scalar fields. The spontaneous breaking of the global U(1) lepton number symmetry leads to the occurrence of a Goldstone boson, the Majoron J, which couples only to right-handed neutrinos and which may have large couplings to the Higgs bosons. The singlet field can generate mass terms for neutrinos.

The DELPHI detector and its performance are described in detail in [9,10]. Analyses of hadronic and muon pair channels are described in sections 2 and 3, respectively. The results are interpreted in section 4.

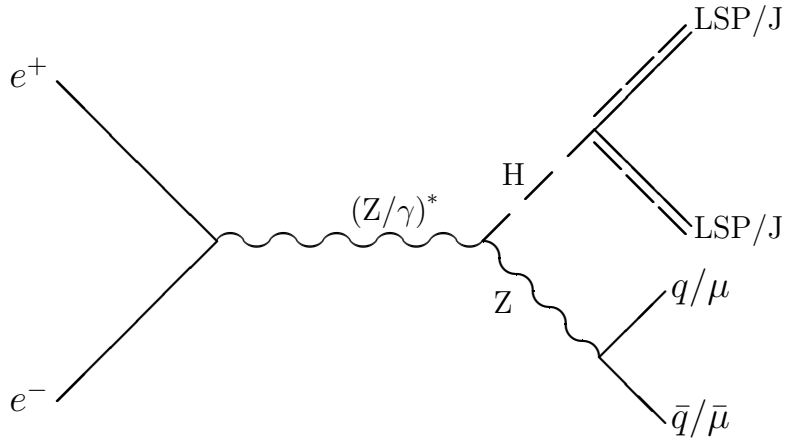

Figure 1: Feynman graph describing the signal process, in which the Higgs particle decays into two lightest supersymmetric particles or two Majorons.

2 Hadronic channel

At $\sqrt{s} \simeq 183$ GeV, the cross-section for the HZ production varies from 1.0 pb for $m_{\mathrm{H}} = 60$ GeV/c^2 to 0.21 pb for $m_{\mathrm{H}} = 90$ GeV/c^2, and 70% of the Z decays into hadronic final states. The signature of an invisible Higgs boson decay is a pair of acoplanar and acollinear jets with a mass compatible with the Z mass, and a missing energy and momentum of the invisible decay.

The data sample corresponds to an integrated luminosity of 50.6 pb^{-1} which satisfies the detector quality status criteria applied in this analysis. The background process $\mathrm{e^+e^-} \to \mathrm{f\bar{f}}(n\gamma)$ and processes leading to four-fermion final states $(\mathrm{Z}/\gamma)^*(\mathrm{Z}/\gamma)^*$, $\mathrm{W^{+*}W^{-*}}$, $\mathrm{We}\nu_\mathrm{e}$ and $\mathrm{Ze^+e^-}$ were simulated using the Monte Carlo generator `PYTHIA` [11], whilst the `TWOGAM` program [12] was used to describe the two-photon interactions. The simulated signal samples were prepared with the `HZHA` program [13]. For this analysis, samples of Higgs boson masses between 60 and 90 GeV/c^2 in 5 GeV/c^2 steps were used. Both signal and background events were processed through the full DELPHI detector simulation and reconstruction programme.

2.1 Particle and event selection procedure

Event variables were computed using reconstructed particles that satisfy the following criteria. Charged particles were defined as reconstructed tracks with momenta above 100 MeV/c, extrapolating to within 4 cm from the primary vertex in $R\phi$ and within 10 cm in z. Neutral particles were defined either as calorimeter showers without associated tracks or as interaction or decay vertices in the tracking volume (e.g. converted photons and V particles). The low-energy thresholds depended on the type of particle with the minimum at 100 MeV.

The event topology of the signal channel resembles the $\mathrm{H}\nu\bar{\nu}$ channel analysed in [17], therefore similar event variables were used, except that no beauty flavour signature was required. The main kinematic variables are the estimated energy of a photon radiated in the beam direction E_γ (normalized to the expected energy of a photon recoiling against a real Z), the total visible energy E_vis, the thrust value in the rest system T_r and the scaled acoplanarity $\log_{10}\theta_\mathrm{acop}$. In order to enhance the discrimination against $\mathrm{W^+W^-}$ events, the missing transverse momentum $\not{p}_\mathrm{T}$, the acollinearity, the largest transverse momentum between any particle and a jet, and the smallest jet mass of the event were used. For the last two variables, the particles were clustered in jets with the `LUCLUS`[11] routine, with the default scaled invariant mass parameter $y_\mathrm{join} = m^2_\mathrm{min}/E^2_\mathrm{vis} = 0.05$. Acollinearity and acoplanarity were defined as 180 degrees minus the angle between the two main jet directions in space, and in the plane transverse to the beam, respectively. The acoplanarity was then multiplied by the sine of the polar angle of the jet closest to the beam (scaled acoplanarity).

The iterated nonlinear discriminant analysis program (IDA) [14] was applied to calculate a second-order polynomial of event variables, thirteen in total. The polynomial specifies a surface which maximizes the separation between signal and background in the event variable space, and its values can be used as weights for signal events.

2.2 Preselections

Preselections were defined in three steps A, B and C. The agreement between the data and the simulation was checked at each step.

A: To select multihadronic annihilation events, the following criteria were applied

- the number of charged particles should be at least nine;
- one or more tracks should extrapolate back to within 200 μm of the event vertex, in the plane transverse to the beam axis. The event vertex was calculated using

good quality tracks with the additional constraint of beam spot determined by the beam position monitors and the event vertices of proximate events;

- the total energy carried by charged particles should be greater than 0.1 $E_{\rm cms}$, and the visible mass should exceed 50 GeV/c^2.

B: Photon hermeticity
A veto algorithm based on the hermeticity counter signals was applied in order to reject events with an on-shell Z and missed or poorly reconstructed photons at large polar angles. These scintillator counters are installed at polar angles of 90 degrees (the connection between two detector hemispheres) and 40 degrees (the gap between the barrel and forward electromagnetic calorimeters) where a photon can escape undetected. The rate of hadronic events of this type is about 1.5 pb. In the final selection, the algorithm reduces the residual background of 3.5±0.2 events of this kind to 0.8±0.1 events, with a relative loss of 6% in the signal efficiencies.

C: Signal region preselection
A loose selection based on the most discriminant variables was applied to define the signal region. The ratio of expected signal and background is of the order of 0.05 after this step. The requirements are listed in table 1.

The agreement between the data and the simulation rates after each preselection step is shown in table 2; the corresponding signal efficiencies are shown in table 3. The data and simulation rates agree within about 5% after steps A and B. The distributions of several event variables are shown for step C in figure 2. The observed and expected rates are within 1.5 σ of each other after step C. The systematic uncertainties quoted in the final hadronic selection will be described in section 2.4.

Variable	min	max
$\not{p}_{\rm T}$	-	60 GeV/c
$M_{\rm vis}$	-	103 GeV/c^2
Acollinearity	10°	85°
$P_{\rm isol}$	-	42 GeV/c
$\log_{10}\theta_{\rm acop}$	0.6	-
$T_{\rm r}$	0.83	-

Table 1: Hq$\bar{\rm q}$ channel: minimum and maximum permitted values in preselection C. $M_{\rm vis}$ is the visible mass, $P_{\rm isol}$ is the momentum of the most isolated particle, other variables are explained in the text.

2.3 Discriminant functions and mass reconstruction

The simulated events passing preselection C were used for calculating the first IDA function which has the distribution shown in figure 3a. At this stage an unbiased comparison of the data and simulation can be made only in the range of the weight variable where the possible signal contribution is negligible. A good agreement between the data and the simulated background is observed. As input for the second iteration a cut was

Selection	Data	Total MC	W^+W^-	$We\nu_e$	$q\bar{q}\gamma$	ZZ^*	Ze^+e^-	$\gamma\gamma$+Bhabha
Step A	6246	6156 ±21	691.8±0.6	17.7±0.1	4918±1	46.1±0.2	36.7±0.9	450±20
Step B	5974	5879 ±21	642.4±1.4	16.8±0.1	4725±3	44.1±0.4	34.5±1.0	420±20
Step C	244	222 ±5	61.1±1.4	11.2±0.2	122.5±1.2	3.6±0.2	1.0±0.3	23±5
1st IDA	35	40 ±1	22.0±0.9	7.0±0.2	8.1±0.3	2.5±0.2	0.0	0.0
Final	13	10.5±0.5	5.1±0.4	2.7±0.1	1.4±0.1	1.4±0.1	0.0	0.0

Table 2: $Hq\bar{q}$ channel: data and simulated background rates after different steps of the analysis.

Selection	Efficiency [%] for different m_H (GeV/c^2)						
	60	65	70	75	80	85	90
Step A	94.9	93.6	93.9	93.3	92.6	93.1	90.9
Step B	88.5	87.5	86.4	85.7	84.8	86.3	84.1
Step C	70.4	70.6	70.9	68.6	66.6	67.4	52.9
1st IDA	56.9	61.0	61.3	63.0	61.0	62.0	47.9
Final	24.4	30.5	35.9	40.3	43.3	44.2	27.7
±(stat.)	1.4	1.5	1.5	1.6	1.6	1.6	1.4
±(syst.)	2.4	3.1	3.6	4.0	4.3	4.4	2.8

Table 3: $Hq\bar{q}$ channel: signal efficiencies after different steps of the analysis.

applied keeping 90% of the signal. The distribution of the weight after the second iteration is shown in figure 3b. The weight distributions as well as the signal and background estimates are obtained from simulation samples that are statistically independent from the samples used in computing the IDA functions.

The invariant mass of the invisible system, the recoil mass, was determined by requiring energy and momentum conservation and by constraining the invariant mass of the visible system to the Z mass. The recoil mass is thus expressed as:

$$M_{rec} = \sqrt{\left(E_{cms} - \frac{m_Z E_{vis}}{M_{vis}}\right)^2 - \left(\frac{m_Z \not{p}}{M_{vis}}\right)^2},$$

where $\not{p}$ is the missing momentum. The distributions of the second weight function versus the recoil mass are shown in figure 4a for the data and in figure 4b for the expected background. The data are in agreement with the prediction from background simulation and no structure is observed in the recoil mass distribution, shown in figure 4c.

The minimum value required for the second IDA weight function, the working point, was chosen by optimizing the expected exclusion limit (see section 4). The best expected limit was obtained for the working point shown by the dashed and thick lines in figures 3b and 4 a,b, respectively. The distributions of the recoil mass in figure 4c are projected for the events above the working point. The efficiencies and expected number of background events are summarized in tables 2 and 3, together with the observed data.

2.4 Results from hadronic channel

The selected data sample consists of 13 events, with an expected background of 10.5±0.5(stat.)±2.0(syst.). The largest background component in the final selection consists of W^+W^- pairs with one W boson decaying into hadrons and the other one into $\tau\nu$ with a large amount of energy escaping in neutrinos.

The systematic uncertainties in the background are expected to be dominated by the imprecision of the detector simulation in reproducing tails of event variable distributions. These effects were studied by smearing the distributions of reconstructed particle multiplicities in the simulation. The amount of particle level smearing was specified by the small deviations observed between the data and simulation in a high statistics sample of hadronic Z events ($\sqrt{s} = m_Z$) collected in the same experimental conditions. These smearings were applied in particle classes of different type, momentum, and polar angle. A background uncertainty of 20% was estimated in the working point selection. Other sources of systematics are negligible with respect to this value. The systematic uncertainties in the efficiencies were checked using a signal-like event sample of hadron jet topologies which were tagged by the presence of isolated particles (leptons from W^+W^- decays or isolated photons in $q\bar{q}\,(n\gamma)$ events). The event variables were computed using the hadronic systems recoiling against the tag particles and were passed through the selection. The agreement between the data and simulation limits the uncertainties in the signal efficiencies to ± 10% relative.

3 Muon channel

The H$\mu^+\mu^-$represents 3.4% of the HZ final states. The experimental signature of the HZ(Z→ $\mu^+\mu^-$) final states is a pair of acoplanar and acollinear muons, with an invariant mass compatible with the expectation from $Z \to \mu^+\mu^-$ decays. The signal and background simulations were made with the same programs as for the hadronic channel. The analysed data sample corresponds to an integrated luminosity of 53.9 pb^{-1}.

3.1 Particle and event selection

Charged particles were selected with similar criteria as those in the hadronic channel. Tracks with momenta above 120% of the beam momentum or with large momentum errors ($\delta p/p$ greater than 100%) were rejected. Neutral particles were selected if their energy in the calorimeters was above 100 MeV.

Events were required to have no more than five charged particles. The two fastest particles were taken as lepton candidates and had to have opposite charges and momenta greater than 10 GeV/c. Other charged particles had to have momenta below 5 GeV/c. This recovered HZ(Z→ $\mu^+\mu^-$) events with two muons accompanied by an electron pair coming from the conversion of a final state photon. Cosmic ray events were rejected by requiring an acollinearity of the two lepton candidates greater than 1°. At least one hit in the vertex detector associated with the fastest charged particle was also required in order to reduce triggers caused by cosmic rays. In addition, the energy of charged particles had to be greater than $0.25\sqrt{s}$. At this level, 97.0% of the Bhabha events and 99.8% of the $\gamma\gamma$ events were rejected.

Muon identification was performed for the two fastest particles in the event to reduce Bhabha and 4-fermions background further. The identification was provided primarily by the algorithm described in [10] which relies on the association of charged particle tracks to signals in the barrel and forward muon chambers. The same algorithm has been extended to the surrounding muon chambers. The longitudinal profile of the energy deposition in the hadron calorimeter was also considered, including the cathode read-out information, in order to improve the identification efficiency. The performance of the muon identification at $\sqrt{s}$ =183 GeV was cross-checked using simulated $Z \to \mu^+\mu^-(\gamma)$ and $Z \to \tau^+\tau^-(\gamma)$ events. After the muon identification, the dominant background comes from $\mu^+\mu^-(\gamma)$ and $\gamma\gamma \to \mu^+\mu^-$ processes. No Bhabha events survive.

Two thirds of the remaining two-photon processes are suppressed by selecting a momentum of the faster muon greater than 41 GeV/c, and lower than 74 GeV/c. Then, the visible mass of the event was required to lie between 79 GeV/c^2 and 96 GeV/c^2. At this level of selection, the dominant background consists of $\mu^+\mu^-\gamma$ events with a photon radiated along the beam pipe. The two-fermion and two-photon backgrounds were suppressed after rejecting events with an acoplanarity of the muon pair with respect to the beam axis below 1.45°. The acollinearity of the muon pair must also be larger than 2.3° and below 62°. The sum of the momenta in the plane transverse to the beam axis was required to be greater than 31 GeV/c. The missing momentum had to be greater than 12 GeV/c and below 51.5 GeV/c, and its direction had to deviate from the beam axis by more than 4.5° .

The above requirements were obtained by a step-wise optimization in which each cut value is varied at a given efficiency in search of the minimum background, iterating over the variables until a stable selection is achieved. The optimization was performed on half of the simulated samples and the selection was then applied to the remaining half to define unbiased efficiency and background estimates. Higgs boson masses from 60 to 95 GeV/c^2 were considered in the optimization. The working point, i.e. the optimal combination of efficiency and background, was determined by minimizing the expected limit, see section 4.

3.2 Results from muon channel

Table 4 details the effect of the selections on the data and the simulated samples contributing to the background. The agreement of the data with the simulation was satisfactory after cosmic ray rejection. This can also be seen in figure 5, which shows the distributions of the acoplanarity and the acollinearity of the two lepton candidates after the cosmic ray rejection, the momentum of the fastest muon, and the visible mass of the event after the muon identification. At the end of the analysis, the expected background comes mainly from W^+W^-, and amounts to $1.74 \pm 0.25(\text{stat.}) \pm 0.59(\text{syst.})$ events. The signal efficiencies for different Higgs boson masses are given in table 5.

Two events were left in the data after the final selection, compared to 1.74 expected from the simulation. In both events, the two muons are clearly identified in the barrel muon chamber and by the cathode readout of the hadron calorimeter. The kinematical variables of these events are shown in table 6.

The systematic uncertainties on the number of events expected for the signal and background were estimated by smearing the selection criteria by amounts corresponding

Selection	Data	Total background	W^+W^-	ZZ^*	$\mu^+\mu^-(\gamma)$ $\tau^+\tau^-(\gamma)$	Ze^+e^- $We\nu_e$	$\gamma\gamma$	Bhabha	$H\mu^+\mu^-$ $\varepsilon(\%)$
Anti-cosmics	3035	3091 ± 13	52.1	2.57	337	10.9	630	2056	86.1
μ identification	402	408 ± 4	11.8	1.26	230	4.76	160	0	83.2
Lepton momenta	143	143 ± 3	9.50	0.94	101	2.45	29.7	0	80.4
Dimuon mass	49	51.2 ± 1.5	2.14	0.20	45.6	0.87	2.39	0	66.1
Event shape	3	2.98 ± 0.35	1.42	0.15	1.12	0	0.30	0	63.4
Miss. momentum	2	1.74 ± 0.25	1.24	0.15	0.35	0	0	0	63.2

Table 4: $H\mu^+\mu^-$ channel: effect of the selections on data, simulated background, and simulated signal events at $\sqrt{s} = 183$ GeV. Efficiencies are given for an m_H=80 GeV/c^2 simulation. The zero quantities have been cross-checked by ignoring the muon identification cut with no new entries at the end.

Efficiency [%] for different m_H (GeV/c^2)							
60	65	70	75	80	85	90	95
34.1 ± 1.0	52.8 ± 1.1	58.5 ± 0.7	59.8 ± 1.0	63.2 ± 1.0	62.0 ± 0.7	59.1 ± 0.7	37.0 ± 1.0

Table 5: $H\mu^+\mu^-$ channel: efficiency of the selection at $\sqrt{s} = 183$ GeV as a function of the mass of the Higgs boson. The uncertainties are due to simulation statistics.

	$p(\mu_1)$ GeV/c	$p(\mu_2)$ GeV/c	Acollinearity $^\circ$	Acoplanarity $^\circ$	p_{mis} GeV/c	θ_{mis} $^\circ$	$M_{vis}(fit)$ GeV/c^2	$M_{miss}(fit)$ GeV/c^2
Event 1	57.2	41.2	44.1	64.1	39.8	70	90.0 ± 2.7	74.9 ± 4.3
Event 2	64.2	32.2	10.4	15.9	32.7	88	91.4 ± 2.7	79.7 ± 5.1

Table 6: $H\mu^+\mu^-$ channel: the selected events. Columns $p(\mu_1)$ and $p(\mu_2)$ are the muon momenta. Columns p_{mis} and θ_{mis} are the missing momentum and polar angles of the missing momentum vectors, respectively. $M_{vis}(fit)$ and $M_{miss}(fit)$ are the fitted invariant masses of the visible and recoil systems, respectively.

to the differences between the mean values of the data and simulation distributions of the event variables. In order to have further sensitivity to generator level effects, the four-fermion processes obtained with the PYTHIA and EXCALIBUR [16] generators were compared at each step of the selection. A systematic uncertainty of ± 0.59 events in the expected background at the working point was assigned, which includes effects from efficiency uncertainties.

4 Interpretation

A confidence level method was used for optimizing the working points and deriving the limits. The confidence at which the signal hypothesis can be rejected (CL_s) was calculated with the technique of modified frequentist likelihood ratio [15], using the reconstructed recoil mass distributions as the event statistic. In this procedure, working points of the two non-overlapping channels $\mathrm{Hq\bar{q}}$ and $\mathrm{H}\mu^+\mu^-$were chosen by maximizing the expected limit. The observed rates of events and their recoil mass distributions were then combined for cross-section and mass limits at the 95% CL_s. The DELPHI 161-172 GeV results of event counting in the hadronic channel [1] were included in the likelihood ratio. These data sets correspond to an integrated luminosity of 19.7 pb^{-1}. One event was observed with an expected total background of 2.2 events and with signal efficiencies in the 14-25% range.

4.1 Cross-section limit

The observed and expected upper limits on the cross-section for the process $\mathrm{e^+e^-} \rightarrow$ Z(anything)H(invisible) were calculated as a function of the Higgs mass. This model-independent result is shown in figure 6a. From the comparison with the SM Higgs boson cross-section and assuming a branching fraction of the Higgs boson into invisible particles, $\mathrm{BR_{inv}}$=100 %, the expected and observed lower mass limits are 80.9 GeV/c^2 and 76.1 GeV/c^2, respectively.

The invisible branching fraction can be assumed to be a free parameter while keeping the relative SM decay probabilities for the visible decays. In this case, the searches for visible and invisible Higgs bosons can be combined, and the excluded region in the ($\mathrm{BR_{inv}}, m_{\mathrm{H}}$) plane is determined assuming SM production cross-sections. Using the DELPHI limits on the visible cross-section [17] a lower mass limit of 76.1 GeV/c^2 is found, independent of the fraction of invisible decays, as is apparent from figure 6b. In computing these limits, the overlap between the Standard Model $\mathrm{H}\nu\bar{\nu}$ and the invisible Higgs boson hadronic selections have been resolved, by using only one at the time: the invisible hadronic mode in the region $BR_{inv} > 50\%$, and $\mathrm{H}\nu\bar{\nu}$ in the region $\mathrm{BR_{inv}} < 50\%$.

4.2 MSSM parameter space exclusion

In the MSSM the Higgs sector is extended to two isodoublets of scalar fields. This leads to the existence of five physical Higgs particles: two CP-even bosons h and H, one CP-odd boson A, and two charged Higgs particles $\mathrm{H}^{\pm}$. The h boson, being the lightest of these five, may be accessible at LEP2 energies.

The MSSM parameters describing the branching ratio of h into invisible states are $\tan\beta$, the ratio of the Higgs field vacuum expectation values, the gaugino mass parameter M_2, assumed to be unified with the mass term M_1, and the Higgs mixing parameter μ. In addition to the kinematical constraints, i.e. the Higgs and neutralino masses, weak isospin conservation in the Higgs boson decay requires that the LSPs are not pure Higgsino or gaugino states, and therefore the branching ratio into neutralinos is largest at $M_2 \simeq |\mu|$. For small $\tan\beta$, the decay of the lightest Higgs boson into a pair of LSPs is favoured, leading to invisible final states. In fact, it turns out that whenever the parameters allow an invisible decay, the branching ratio is likely to be near 100%. The MSSM h boson production cross-section is proportional to the SM Higgs boson cross-section with a ratio $\sin^2(\beta-\alpha)$. The mixing parameter α is defined by $m_{\rm Z}$, $m_{\rm A}$ and $\tan\beta$.

The program HDECAY[18] was used to calculate the branching ratio for the lightest Higgs boson into LSPs. Assuming $\tan\beta = 1.65$ and $m_A = m_{\rm Z}$ a scan can be made over the two remaining parameters M_2 and μ. A point in the MSSM parameter space is excluded if it satisfies the requirement

$$\sigma(\mathrm{h} \rightarrow \mathrm{inv}\ ) = \sigma_{\rm SM}(\mathrm{hZ}) \cdot \sin^2(\beta-\alpha) \cdot \mathrm{BR}(\mathrm{h} \rightarrow \mathrm{inv}\ ) > \sigma(\mathrm{limit})$$

The 95% CL excluded region, with the specified parameter values, is shown in figure 6c. The parameter region overlaps the exclusion region from direct searches for charginos and neutralinos [6].

4.3 Majoron model

The cross-section limits can be used to set a limit on the Higgs bosons in a Majoron model with one Higgs boson doublet ϕ and one singlet η [7,8]. Mixing the real parts of ϕ and η leads to two massive Higgs bosons:

$$\mathrm{H} = \phi_{\rm R}\ \cos\theta - \eta_{\rm R}\ \sin\theta$$

$$\mathrm{S} = \phi_{\rm R}\ \sin\theta + \eta_{\rm R}\ \cos\theta,$$

where θ is the mixing angle. The imaginary part of the singlet field is identified as the Majoron which decouples from the fermion and gauge sector but might have large couplings to the Higgs bosons. The free parameters of this model are the masses of the two Higgs bosons (H and S), the mixing angle θ, and the ratio of the vacuum expectation values of the ϕ and η fields ($\tan\beta \equiv v_\phi/v_\eta$).

The production rates of the H and S are reduced with respect to the SM Higgs boson by factors of $\cos^2\theta$ and $\sin^2\theta$ respectively. The decay widths of the H and S into the heaviest possible fermion-antifermion pair are reduced by the same factor and their decay widths into a Majoron pair are proportional to the complementary factors ($\cos^2\theta$ for S and $\sin^2\theta$ for H). We concentrate on the case where the invisible Higgs boson decay mode is dominant ($\tan\beta$ large). The excluded region in the mixing angle versus Higgs boson mass plane is shown in figure 6d.

5 Conclusion

In a data sample of 54 pb^{-1}collected by the DELPHI detector at centre-of-mass energies of $\sqrt{s} \simeq 183$ GeV two H$\mu^+\mu^-$ candidates were found with an expected background

of 1.7±0.2(stat.)±0.2(syst.) events, and 13 Hq$\bar{\text{q}}$ events were selected with an expected background of 10.5±0.5(stat.)±2(syst.) events.

Combining these analyses and the earlier DELPHI LEP2 results, the mass limit for Higgs bosons is 76.1 GeV/c^2 with a Standard Model cross-section. This limit is valid for an arbitrary fraction of invisible Higgs boson decays. In the Majoron model with one doublet and one singlet, a large region in the Higgs boson mass versus the mixing angle plane is excluded beyond the reach of LEP1.

Acknowledgements

We are greatly indebted to our technical collaborators, to the members of the CERN-SL Division for the excellent performance of the LEP collider, and to the funding agencies for their support in building and operating the DELPHI detector.
We acknowledge in particular the support of
Austrian Federal Ministry of Science and Traffics, GZ 616.364/2-III/2a/98,
FNRS–FWO, Belgium,
FINEP, CNPq, CAPES, FUJB and FAPERJ, Brazil,
Czech Ministry of Industry and Trade, GA CR 202/96/0450 and GA AVCR A1010521,
Danish Natural Research Council,
Commission of the European Communities (DG XII),
Direction des Sciences de la Matière, CEA, France,
Bundesministerium für Bildung, Wissenschaft, Forschung und Technologie, Germany,
General Secretariat for Research and Technology, Greece,
National Science Foundation (NWO) and Foundation for Research on Matter (FOM), The Netherlands,
Norwegian Research Council,
State Committee for Scientific Research, Poland, 2P03B06015, 2P03B03311 and SPUB/P03/178/98,
JNICT–Junta Nacional de Investigação Científica e Tecnológica, Portugal,
Vedecka grantova agentura MS SR, Slovakia, Nr. 95/5195/134,
Ministry of Science and Technology of the Republic of Slovenia,
CICYT, Spain, AEN96–1661 and AEN96-1681,
The Swedish Natural Science Research Council,
Particle Physics and Astronomy Research Council, UK,
Department of Energy, USA, DE–FG02–94ER40817.

References

[1] DELPHI Collaboration, P. Abreu et al., *Eur. Phys. J.* **C2** (1998) 1.

[2] ALEPH Collaboration, D. Buskulic et al., *Phys. Lett.* **B313** (1993) 549;
"*Search for invisible Higgs boson decays in e^+e^--collisions at centre-of-mass energies up to 184 GeV*", CERN EP/99-008;
L3 Collaboration, M. Acciarri et al., *Phys. Lett.* **B418** (1998) 389;
L3 Collaboration, M. Acciarri et al., *Phys. Lett.* **B385** (1996) 454;
OPAL Collaboration, G. Alexander et al., *Phys. Lett.* **B377** (1996) 273.

[3] H.P. Nilles, *Phys. Rep.* **110** (1984) 1;
H.E. Haber and G.L. Kane, *Phys. Rep.* **117** (1985) 75.

[4] A. Djouadi, P. Janot, J. Kalinowski and P.M. Zerwas, *Phys. Lett.* **B376** (1996) 220.

[5] A. Djouadi and M. Drees, *Phys. Lett.* **B407** (1997) 243;
L.J. Hall et al., *Phys. Lett.* **B424** (1997) 305.

[6] DELPHI Collaboration, P. Abreu et al., *Phys. Lett.* **B446** (1999) 75.

[7] A. Zee, *Phys. Lett.* **B93** (1980) 389.
Y. Chikashige, R.N. Mohapatra and R.D. Peccei, *Phys. Lett.* **B98** (1980) 265;
R.E. Shrock and M. Suzuki, *Phys. Lett.* **B110** (1982) 250;
R. Mohapatra and J.W.F. Valle, *Phys. Rev.* **D34** (1986) 1642;
M.C. Gonzalez-Garcia and J.W.F. Valle, *Phys. Lett.* **B216** (1989) 360;
E.D Carlson and L.J. Hall, *Phys. Rev.* **D40** (1989) 3187.

[8] F. de Campos et al., *Phys. Rev.* **D55** (1997) 1316.

[9] DELPHI Collaboration, P. Abreu et al., *Nucl. Instrum. and Meth.* **A303** (1991) 233.

[10] DELPHI Collaboration, P. Abreu et al., *Nucl. Instrum. and Meth.* **A378** (1996) 57.

[11] T. Sjöstrand, *Comp. Phys. Comm.* **39** (1986) 347;
Comp. Phys. Comm. **82** (1994) 74.

[12] S. Nova et al., in CERN Report 96-01, Vol. 2, p. 224.

[13] P. Janot, in CERN Report 96-01, Vol. 2, p. 309.

[14] T.G.M. Malmgren, *Comp. Phys. Comm.* **106** (1997) 230;
T.G.M. Malmgren and K.E. Johansson, *Nucl. Instrum. and Meth.* **A403** (1998) 481.

[15] A.L. Read, "*Optimal statistical analysis of search results based on the likelihood ratio and its application to the search for the MSM Higgs boson at $\sqrt{s}$ = 161 and 172* GeV", DELPHI 97-158 PHYS 737.

[16] F.A. Berends, R. Pittau and R. Kleiss, *Comp. Phys. Comm.* **85** (1995) 437.

[17] DELPHI Collaboration, P. Abreu et al., "*Search for neutral Higgs bosons in e^+e^- collisions at $\sqrt{s}$ =183 GeV*", accepted for publication in *Eur. Phys. J. C.*

[18] A. Djouadi, J. Kalinowski, M. Spira, *Comp. Phys. Comm.* **108** (1998) 56.

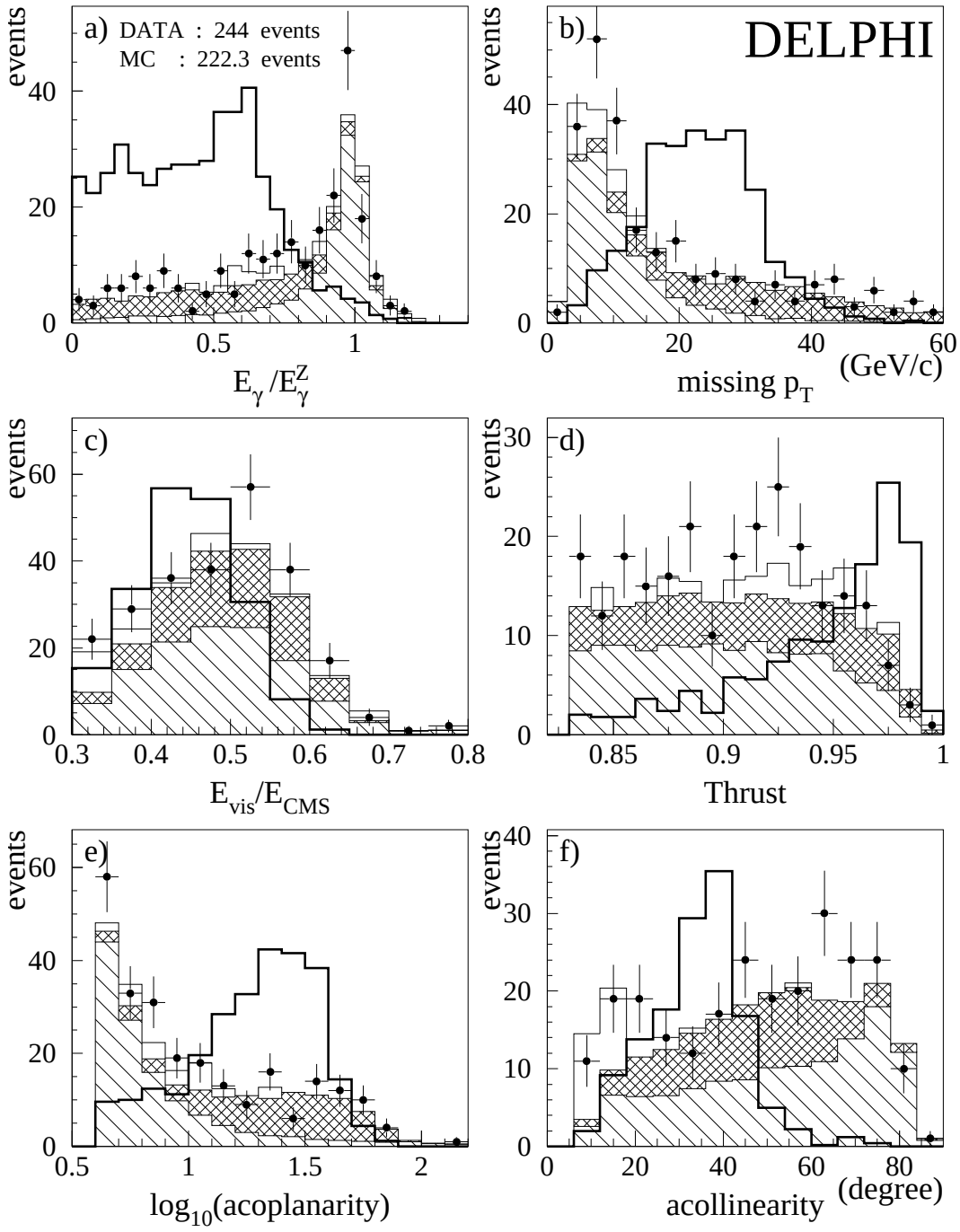

Figure 2: A comparison of data (dots) and simulated background for the six variables, defined in the text, in the Hq$\bar{\text{q}}$ channel after preselection C. The thin histogram line is the sum of q$\bar{\text{q}}\gamma$ (hatched), 4-fermion background (double hatched), $\gamma\gamma$ and a small contribution from Bhabha processes. The thick line is the expected signal distribution for an 80 GeV/c^2 Higgs boson with arbitrary scale.

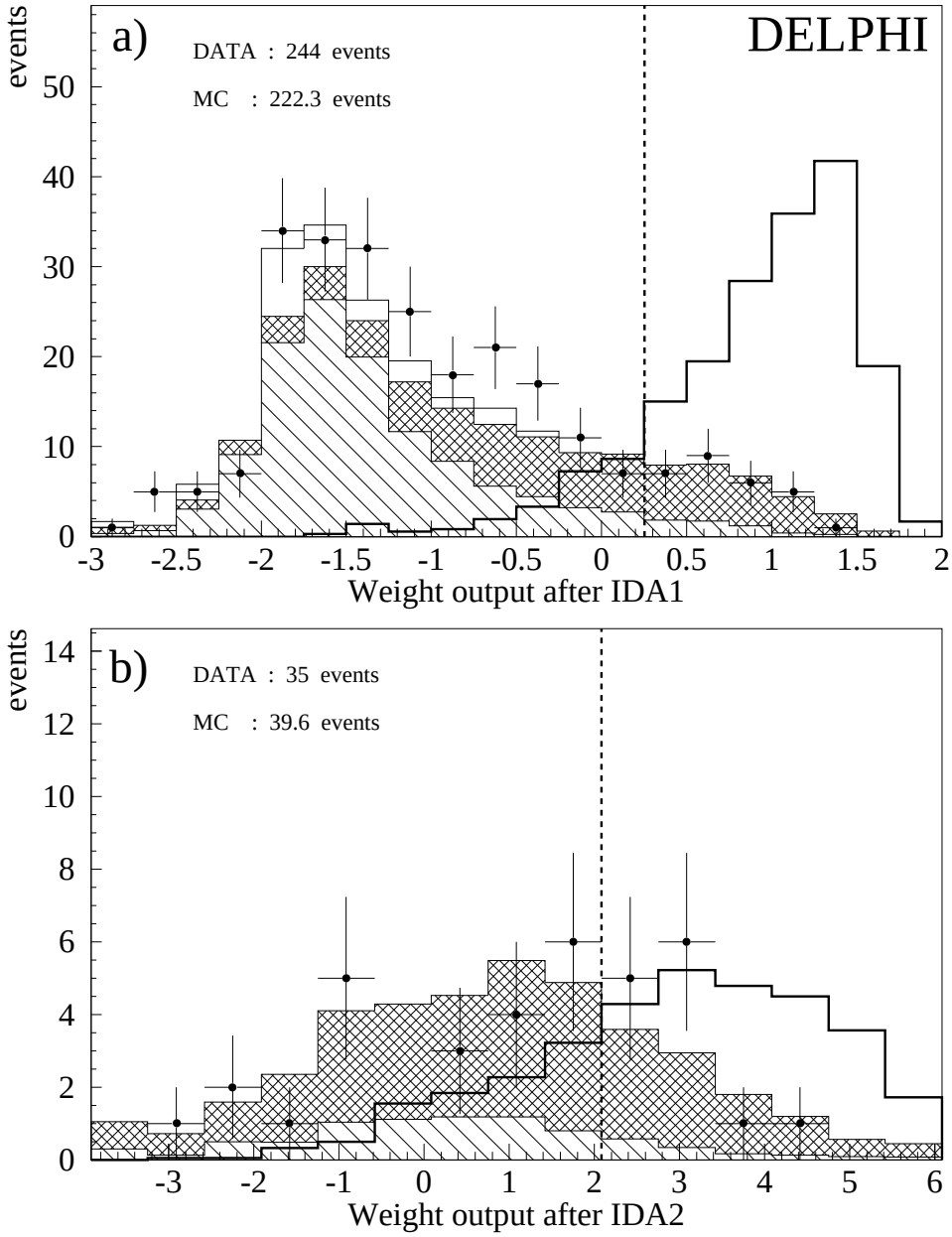

Figure 3: The weight from the first (a) and second (b) step of the iterative discriminant analysis (IDA) for the Hq$\bar{\text{q}}$ channel. The applied cuts are shown as vertical lines. The thick line is the expected signal distribution for an 80 GeV/c^2 Higgs boson, normalized to the luminosity, scaled up by factors of ten and two in (a) and (b), respectively. The dots represent the data and the background is defined as in figure 2.

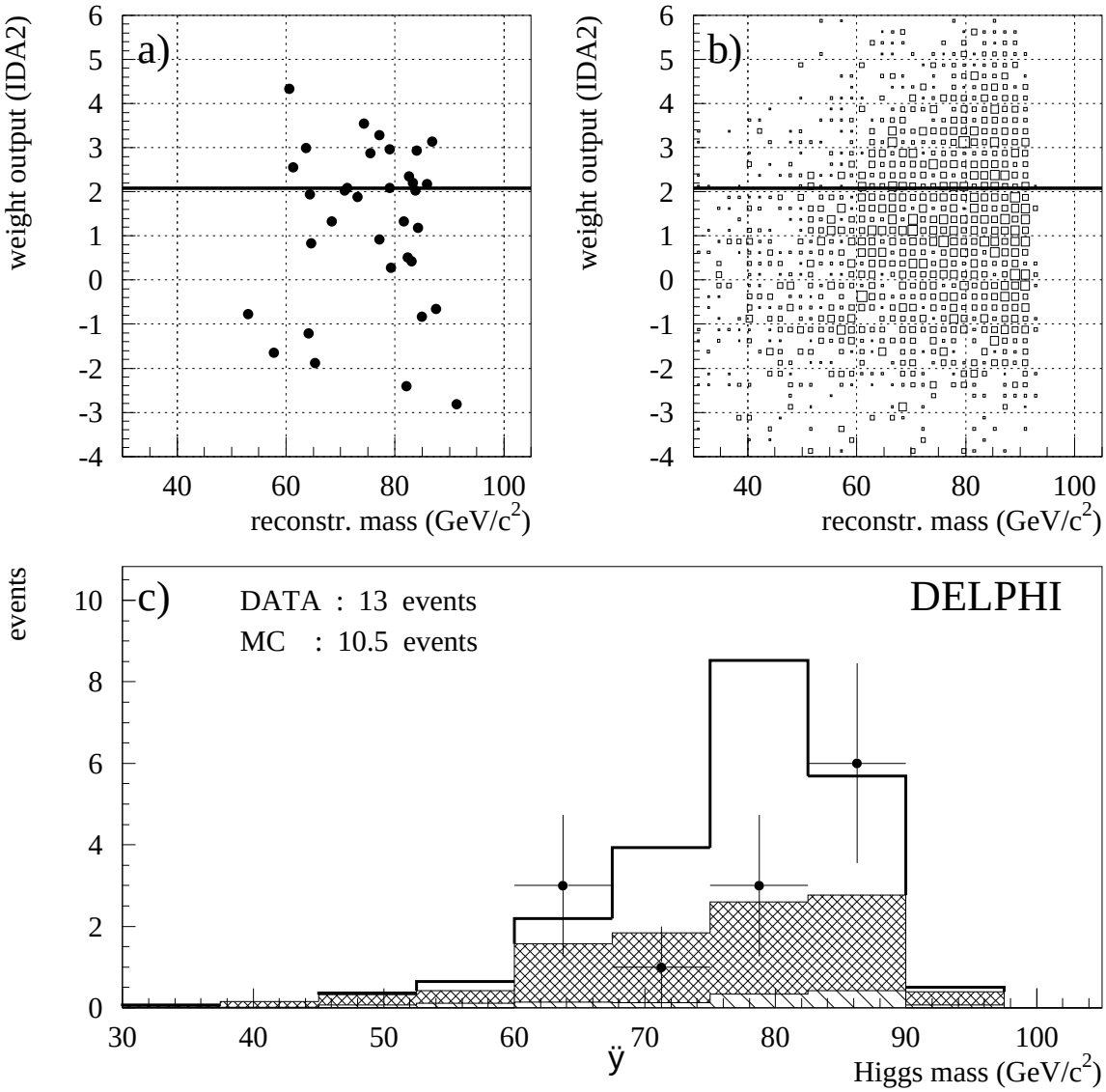

Figure 4: The distributions of the second IDA weight function vs. the recoil mass for the events selected after the first IDA iteration for the data (a) and the background (b), and the distribution of the recoil mass (c) in the working point region above the horizontal line in (a,b). The thick line is the expected signal distribution for an 80 GeV/c^2 Higgs boson, normalized to the luminosity and added on top of the background. The dots represent the data and the background is defined as in figure 2.

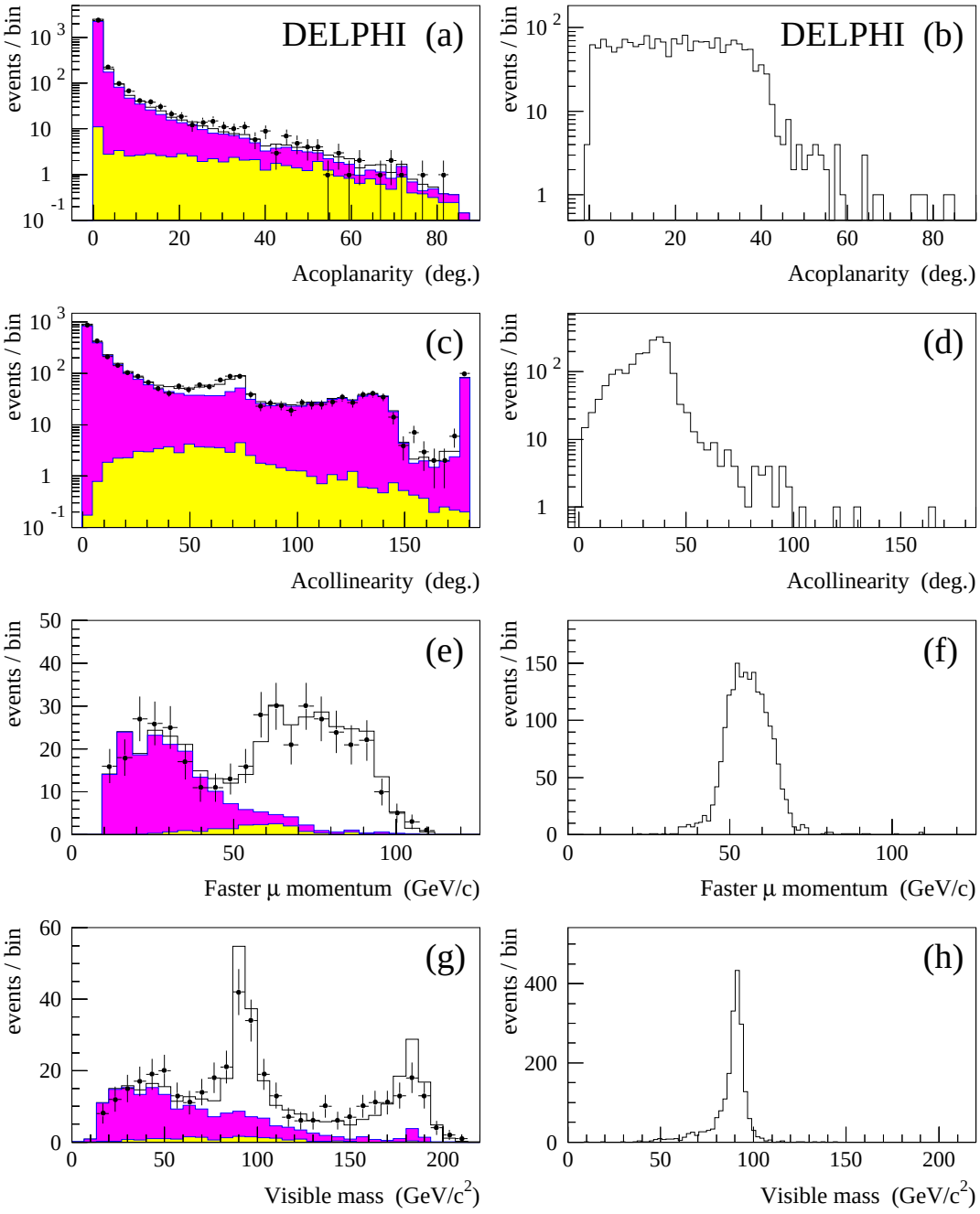

Figure 5: H$\mu^+\mu^-$ analysis: Distributions of the acoplanarity (a-b) and of the acollinearity (c-d) of the two muon candidates after the rejection of cosmic ray events. Distributions of the momentum of the fastest muon (e-f) and of the visible mass (g-h) after muon identification. The plots on the left show a comparison between $\sqrt{s}$ =183 GeV data (points) and simulated background events (solid line) normalized to the experimental luminosity. The light grey area represents the contribution from the 4-fermion background, the dark grey the contribution of Bhabha and 2-photon processes, and the white area the contribution of ll(γ)(DYMU3 generator). The plots on the right show the unnormalized expected distributions for a Higgs boson of 80 GeV/c^2.

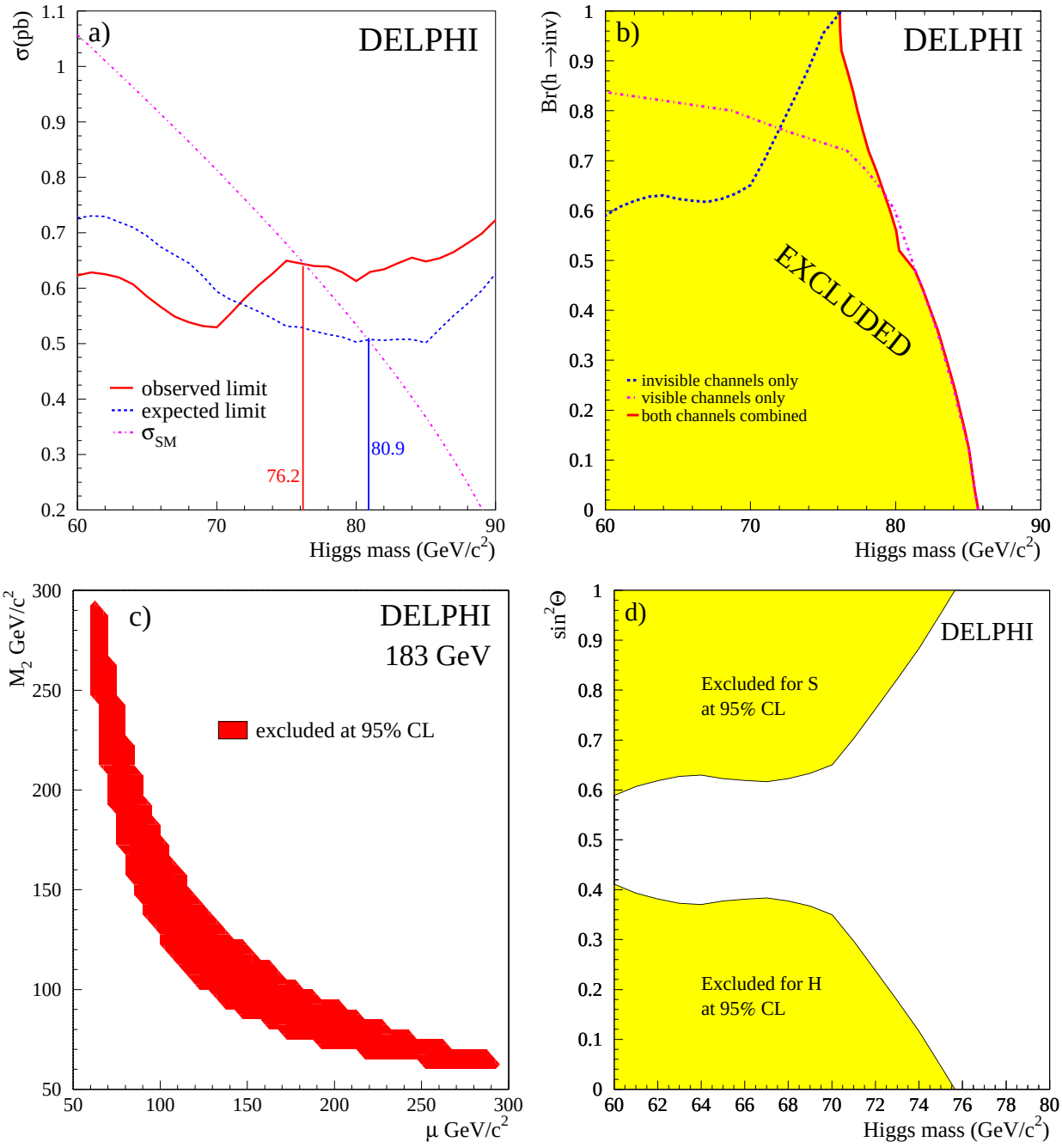

Figure 6: a) The 95% CL upper limit on the cross-section of the process $e^+e^- \rightarrow Z(\text{anything})\,H(\text{invisible})$ as a function of the Higgs boson mass. The dashed-dotted line shows the Standard Model cross-section. b) Limits on $m_H$as a function of the branching ratio into invisible decays, assuming a $(1 - BR)$ branching ratio into standard visible decay modes. c) Excluded area in the MSSM M_2 vs. μ plane for $m_A = m_Z$ and $\tan\beta = 1.65$. d) Limit on $\sin^2\theta$ as a function of the Higgs boson mass at 95% CL. S and H are the Higgs bosons in the Majoron model with expected production rates for large $\tan\beta$. In this case, the Higgs boson decays only invisibly.